High-Power Indium Phosphide Photonic Integrated Circuits

Hongwei Zhao ⓘ, Sergio Pinna, Fengqiao Sang, Bowen Song, Simone Tommaso Šuran Brunelli,
Larry A. Coldren ⓘ, *Life Fellow, IEEE*, and Jonathan Klamkin, *Senior Member, IEEE*

(Invited Paper)

Abstract—Indium phosphide (InP) is the most developed platform for photonic integrated circuits (PICs). Of interest is the advancement of this platform for applications that demand high performance, especially high output power, including free space communications and microwave photonics. In this paper, we summarize development of InP-based PIC transmitters. Two transmitter types were fabricated: one based on an offset quantum wells (OQW) platform and the other on a quantum well intermixing (QWI) platform. The OQW-based transmitter consists of a widely tunable laser, a high-speed semiconductor optical amplifier (SOA), a Mach–Zehnder modulator, and an output SOA. This transmitter demonstrates a 44-nm tuning range, >45 dB side mode suppression ratio, 14.5 dBm OFF-chip power, and a data rate of 7 Gbps. The second transmitter, based on QWI, utilizes an alternate epitaxial structure to achieve a lower confinement factor for higher SOA output saturation power. This QWI transmitter consists of a distributed Bragg reflector laser, a high-speed SOA, an electroabsorption modulator, and an output SOA. The measured OFF-chip power is 19.5 dBm, and a data rate of 20 Gbps is demonstrated. Based on the improved performance with the new epitaxial structure, a novel platform for high-power PIC transmitters integrated with low confinement and high-power SOAs is described.

Index Terms—Photonic integrated circuits, DBR laser, optical transmitter, sampled grating DBR laser, semiconductor optical amplifier, offset quantum wells, quantum well intermixing, free space optics.

I. INTRODUCTION

INDIUM phosphide (InP) is the most advanced platform for high-performance large-scale photonic integrated circuits (PICs). This platform allows for the monolithic integration of all the required active elements (e.g., lasers, semiconductor optical amplifiers (SOAs), modulators, photodetectors), and passive components (e.g., waveguide interconnects, filters, couplers), thus enabling complex single-chip implementations

of advanced transmitters and receivers. Compared to optical systems with discrete components, monolithic integration improves the system reliability and provides significant reduction in packaging cost, system footprint, fiber coupling loss and power consumption [1]–[3].

High-performance InP-based PICs have been widely used in coherent transmitter, receiver, wavelength-conversion and packet-switching applications [4]–[7]. The last several decades have witnessed the maturation of InP from discrete photonic devices to complex high-functionality PICs. The electroabsorption modulated laser (EML) was first introduced in mid-1980s [8]. This device integrated a three-section distributed Bragg reflector (DBR) laser with an electroabosprtion modulator (EAM). Distributed feedback (DFB) lasers were also incorporated into EMLs and this two-component device has become a mainstay in telecommunications, providing benefits over the use of separate discrete components [9]. Widely tunable laser sources were developed for wavelength division multiplexing (WDM) systems, but have also found use in sensing applications. The sampled grating DBR (SGDBR) laser was first proposed in early 1990s. It provides wide optical tuning range without compromising mode suppression [10]–[12]. The first commercial large-scale multi-channel InP PIC transmitter/receiver for dense WDM was reported in 2004 [13]. Since then, advancements have been made in manufacturing capability so as to realize InP PICs with 14-channel coherent transmitter on a single chip for 4.7 Tbps aggregate capacity [14].

In addition to fiber optic communication systems, InP PICs can impact other applications where high performance is required in conjunction with low cost, size, weight and power (CSWaP). These include microwave photonics and free space communications [15]–[18]. For high linearity microwave photonics links, InP coherent receivers were developed demonstrating state-of-the-art spurious-free dynamic range [19]. Widely tunable InP PICs have also been used for optical frequency synthesis and coherent LiDAR [20], [21]. PICs are particularly attractive for free space optical communications where low CSWaP is critical [22]–[25]. The Lunar Laser Communications Demonstration (LLCD) was a highly successful demonstration of laser communications (lasercom) in space [26]. Since the success of this program, several lasercom efforts have been pursued by various space agencies and by industry [27]. Lasercom transmitters are desired to output high peak power levels

and to support power-efficient modulation formats [28], [29]. Although some work has been carried out to realize high-power InP lasers and SOAs [30]–[32], little to no work has been carried out to realize a full high-power InP PIC platform because of the challenges associated with integrating high-confinement waveguides (for seed lasers, modulators, photodetectors, and passives) with low-confinement waveguides (for high-power lasers and SOAs).

In conventional InP PICs, the active waveguide width is typically only 2–3 μm, resulting in mode dimensions on the order of 3 μm $\times$ 1 μm. The small mode size and high confinement factor ($>5\%$) is beneficial to achieve maximum modal gain for lasers and high efficiency for modulators. However, high confinement limits the saturation output power of SOAs. A number of approaches have been employed to improve the SOA saturation power. One is to increase the width of the active region with a flared waveguide [33], [34]. Waveguide SOAs with width of a few hundred microns were reported with output power up to 0.3 W [35]. Since the thickness of the active region is typically 1 μm, the large beam dimension in the horizontal direction imposes challenges on the coupling to single-mode fiber. A second approach is to decrease the confinement factor. The photon density within the active region is reduced with lower confinement, thus decreasing the stimulated emission rate, which slows down the carrier depletion and in turn increases the saturation power. Slab-coupled optical waveguides (SCOW) with small confinement factor ($\sim 0.25\% - 1\%$) have been investigated for high-power SOAs and lasers. Unlike conventional single-mode waveguide SOAs, the SCOW concept expands the mode in the vertical directional and is engineering for single-mode behavior. External-cavity SCOW lasers and SOAs with 29-dBm saturation power have been separately reported [36], [37]. However, it is very challenging to realize monolithic integration of the SCOW SOAs with other optical elements required for a PIC such as a seed laser and modulator.

In this work, we have investigated InP PIC transmitters for high optical power and proposed a novel platform enabling the monolithic integration of low-confinement SOAs with other high-confinement components including a seed laser and high-speed modulator. The first type of InP PIC transmitter presented is based on an offset quantum well (OQW) platform. Although the fabrication process is fairly simple, the performance of the integrated components is limited. It is also challenging to incorporate a dilute waveguide (i.e., an InGaAsP waveguide layer with lower refractive index) into this platform primarily because of the mode discontinuity in the active and passive regions. Nevertheless, OQW InP PICs with seed lasers, modulators, and booster SOAs demonstrated up to 14.5 dBm off-chip power and a 7 Gbps data rate. These PICs were also incorporated into a basic free space transmission experiment and were compared in performance to a transmitter based on high-performance commercial discrete components [15], [29]. A more advanced transmitter was developed based on a quantum well intermixing (QWI) platform. In addition to allowing for the integration of higher efficiency modulators, this platform was adapted to a dilute waveguide structure allowing for the integration of both high-confinement and low-confinement waveguide compo-

nents. The QWI PIC transmitters demonstrated up to 19.5 dBm off-chip output power and a 20 Gbps data rate. In addition to describing the design, fabrication, and characterization results of the OQW and QWI PIC transmitters, a discussion is provided on the implementation and integration of low-confinement, high-power integrated SOAs.

II. HIGH POWER AMPLIFIERS

The optical output power of PICs primarily depends on the performance of the output SOA. The main factors limiting the output power of an SOA are the gain (G) and saturation output power ($P_{o,sat}$). During the amplification process, the carriers in the active gain region become depleted as the optical power increases, resulting in a decrease of the gain and the power saturation. The saturation output power can be expressed as:

$$P_{o,sat} = \left(\frac{G_0 ln2}{G_0 - 2} \right) A \left(\frac{h\nu}{a\tau} \right) \tag{1}$$

where G_0 is the unsaturated gain, $h\nu$ is the photon energy, a is the differential gain, τ is the carrier lifetime, and A is the amplifier modal area [30]. In conventional SOAs, A can be estimated as:

$$A = \frac{wd}{\Gamma} \tag{2}$$

where w and d are the width and thickness of the active material, and Γ is the optical confinement factor. $P_{o,sat}$ is proportional to the modal area, which can be increased by proper design of the waveguide structure in the active layers.

In this work, two different InP-based epitaxial structures (denoted S1 and S2) were investigated for output power considerations, one based on the OQW platform, and the other on an advanced QWI platform that includes a lower dilute waveguide for transitioning a guided optical mode to lower optical confinement. The epitaxial structures were grown by metal organic chemical vapor deposition (MOCVD) on n-type (001) InP substrates. In both structures, the active layers consist of five pairs of indium gallium arsenide phosphide (InGaAsP) quantum wells that are situated above an InGaAsP waveguide (WG) core layer. The layer structures and corresponding fundamental TE modes in a ridge waveguide are shown in Fig. 1 and Fig. 2. Ordinarily a high index waveguide core layer is selected for low threshold high efficiency lasers. For S1, the composition of the InGaAsP WG core layer was selected to achieve a slightly lower index (bandgap wavelength of 1.24 μm), so that the confinement factor is made lower without significant change to the epitaxial layers. For S2, a 2.5-μm thick waveguide layer (WG2) was added below the primarily guiding structure. With the same ridge waveguide width, S2 yields a modal area of 3.37 μm^2, 53% larger than that of S1. The modal area can be significantly increased from this by engineering the waveguide geometry so that the mode mostly couples to the lower waveguide layer WG2.

By tailoring the waveguide geometry, two advanced SOA designs with ultralow confinement ($<1\%$) in the active gain region would enable higher saturation output power. Fig. 3 shows two SOA designs with epitaxial structure S2. As the waveguide width is reduced from 3 μm to 1.5 μm and the
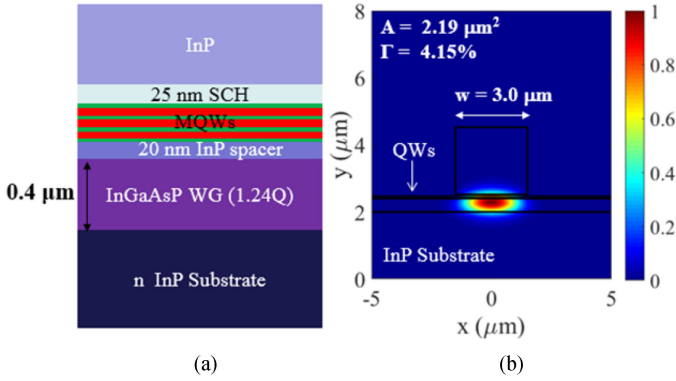
Fig. 1.   (a) Epitaxial structure S1; (b) Fundamental TE mode in a ridge waveguide with S1.
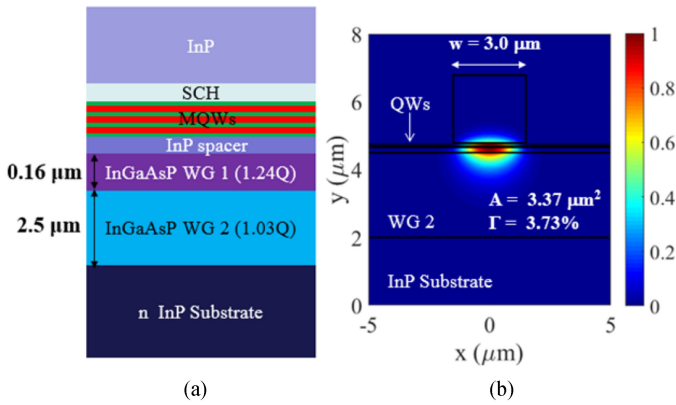

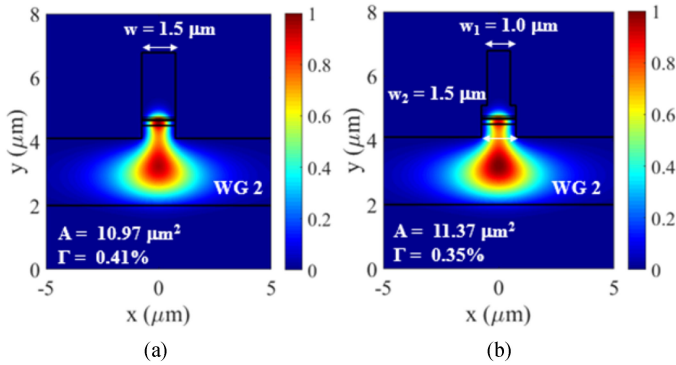Fig. 2.   (a) Epitaxial structure S2; (b) Fundamental TE mode in a ridge waveguide with S2.

Fig. 3.   Fundamental TE mode in advanced waveguide designs with epitaxial structure S2 for ultralow confinement and ultimately high SOA output saturation power. (a) Single-ridge waveguide; (b) Double-ridge waveguide.

ridge is etched into the lower waveguide layer, the confinement is dramatically decreased to 0.41% and the corresponding modal area is increased by a factor of 3.3. A double ridge design would further lower the confinement factor and increase the modal area. This latter structure facilitates the coupling of the optical mode from the high confined regime, where most of the mode is confined in the upper waveguide (WG1), to the

lower confined regime, where most of the mode is confined in the lower waveguide (WG2).

III.   INTEGRATION PLATFORM AND FABRICATION

A high-functionality PIC platform must facilitate coupling between different integrated elements to optimize system performance and reliability. This can be challenging since the design of each element requires unique epitaxial structures and waveguide designs for optimum device performance. High efficiency lasers require a highly confined quantum well structure for large modal gain. Mach-Zehnder modulators (MZMs) based on the Franz-Keldysh effect utilize bulk material. For EAMs, the bandgap of the quantum wells should be blue shifted from that of the laser region to reduce insertion loss. For high saturation power SOAs, a weakly confined optical mode is preferred for lowering the local photon density. To enable complex functions on a single chip, efforts have been made to advance various integration technologies over the past three decades. Integration schemes include selective area regrowth (SAG), butt-joint growth (BJG), OQW, and QWI.

SAG utilizes a patterned dielectric mask to modify the thickness and composition of the epitaxial layers, allowing for varying bandgaps across a wafer [38], [39]. The growth conditions have to be precisely controlled to achieve desired bandgaps.

BJG involves selective removal of as-grown quantum wells, selective regrowth of alternative material structures with desired bandgaps, and then growth of a doped upper cladding [40], [41]. Some such processes include an additional regrowth step to incorporate an unintentionally doped cladding in the passive regions. BJG requires separate complex growth steps for each component thus increases the fabrication complexity and consequently yield problems in the past. Recent investigations on the epitaxial technology have resolved the yield issue with BJG [42], [43].

The OQW platform is simple and robust. It is based on the selective removal of quantum wells in regions where gain is not needed and a single, blanket (i.e., not selective) P-type cladding regrowth [44], [45]. Since this platform allows for only two unique bandgaps, the SOAs must share the same epitaxial layers as the lasers, generally resulting in higher confinement than is not desired for a high power SOA. The composition of the waveguide core also influences the tradeoffs between passive loss, modulator efficiency, and SOA saturation power.

QWI is a post growth technique that can modify the bandgap of quantum wells selectively. The QWI process utilized here is based on ion implantation and annealing to generate point defects in a sacrificial layer and subsequently diffuse these defects into the quantum well region [46], [47]. This process ultimately reshapes the quantum wells and effectively increases the quantum well bandgap. This platform is ideal because it allows for integration of multiple bandgaps while minimizing the index discontinuity at interfaces, the latter of which is important for integration with low confinement waveguides such as that utilized in structure S2.

With epitaxial structure S1, a PIC transmitter was realized by simple OQW platform. Fig. 4 illustrates the OQW-based
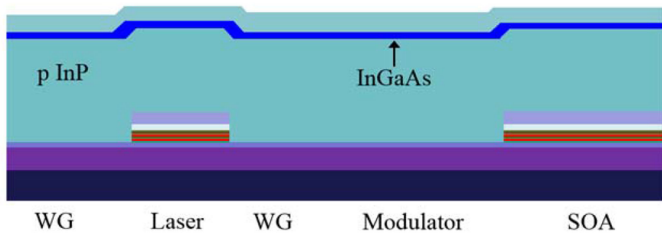
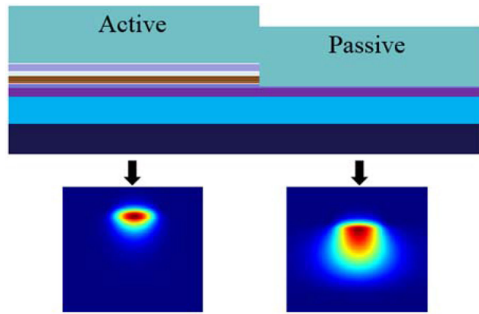Fig. 4.   Schematic of the OQW-based PIC transmitter.

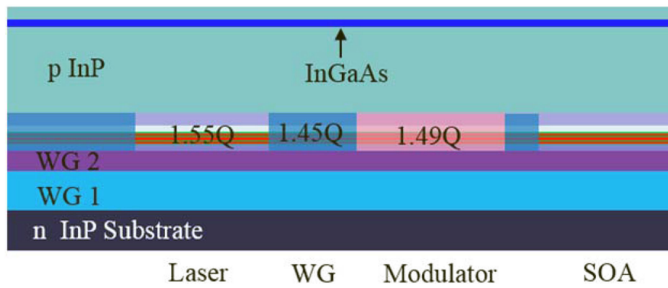Fig. 5.   Active/passive interface of S2 with OQW platform.

Fig. 6.   Schematic of the QWI-based high-power PIC transmitter.

Fig. 7.   Photoluminescence of the different regions in S2.
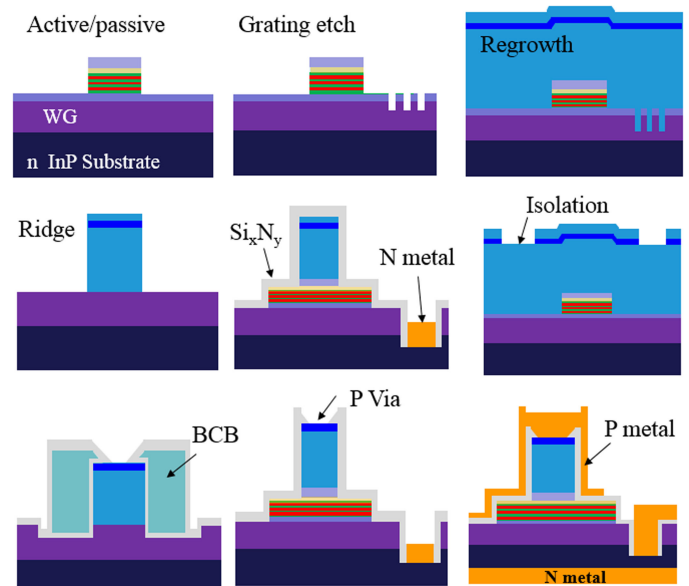
Fig. 8.   Fabrication flow for OQW-based transmitter.

PIC transmitter with S1. The quantum wells outside the gain regions were removed by wet etch. A SGDBR laser design was employed for widely tunable range. Franz-Keldysh absorption based modulator works at reverse bias, as the tilting of the bands increase the tunneling probability when electrical field increases.

Epitaxial structure S2 was optimized with a thick lower waveguide layer (1.03Q) for low confinement in SOA. If OQW platform was used for S2, the active/passive interface will experience significant mode mismatch (as shown in Fig. 5). To reduce the interface discontinuity, QWI platform is preferred. Besides, QWI technique enables efficient EAM, thus eliminate the tradeoff between modulation efficiency and insertion loss.

A schematic of QWI-based high power PIC transmitter is demonstrated in Fig. 6. A two-step anneal process were developed after a single P^+ implantation. The sample was annealed to reach a desire bandgap for efficient electro-absorption modulation, then the InP buffer layer was removed in the modulator region. The bandgap in passive region, where the buffer layer were intact, will be further blue-shifted with additional
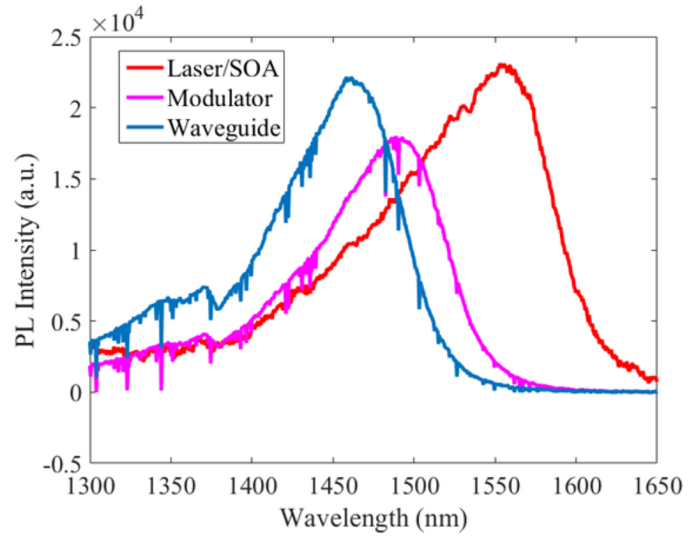
annealing. As shown Fig. 7, PL peaks in the gain section, EAM and passive waveguide are 1550 nm, 1490 nm and 1450 nm, respectively.

The fabrication process for the OQW-based and QWI-based PIC transmitters are similar except for the active/passive definition. The fabrication flow for OQW-based PIC transmitter is shown in Fig. 8. Grating mirrors were patterned by electron beam lithography and dry etched with chlorine-based ion beam etching. This was followed by a 'blanket' regrowth of the InP cladding and p+ InGaAs contact layer. The waveguide ridges were then formed in the [110] direction by using inductively coupled plasma dry etch and a cleanup wet etch to form smooth vertical sidewalls. Topside n-metal (Ni/AuGe/Ni/Au) were deposited. The p+ InGaAs contact layer was removed between
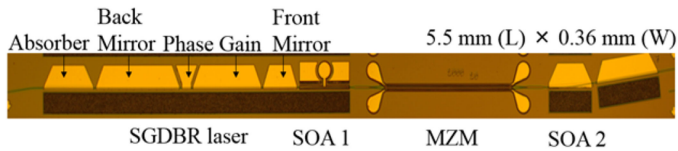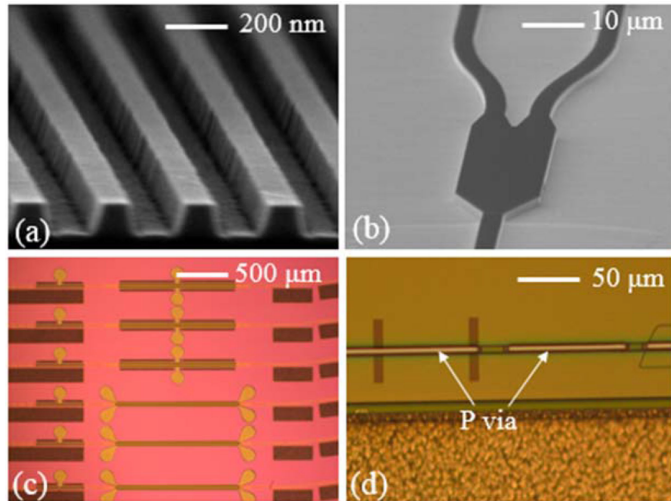
Fig. 9. Microscope image of fabricated OQW-based PIC transmitter.

Fig. 10. Microscope images at various stages of the fabrication process of OQW-based transmitter: (a) The sampled gratings of the front mirror of the laser; (b) Top view of a 1×2 MMI structure; (c) BCB patterns for high-speed SOAs and MZMs; (d) P vias on top of ridges.
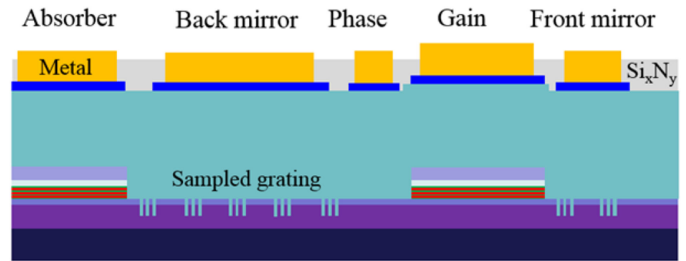

Fig. 11. Schematic of the five-section SGDBR laser.
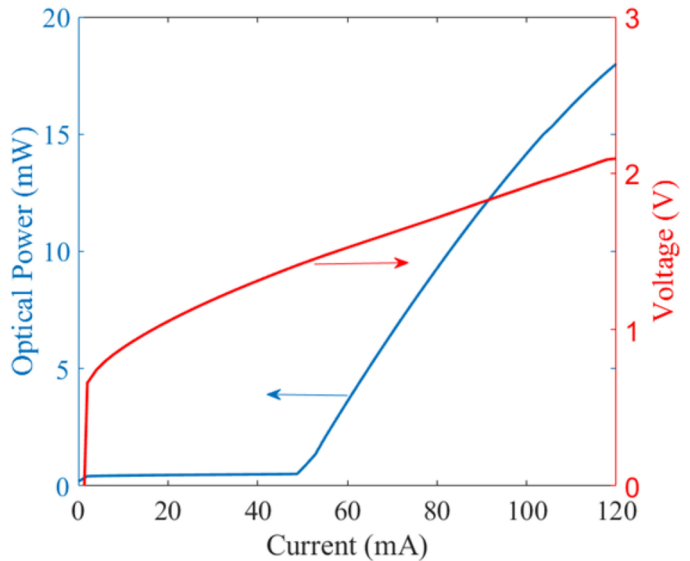
Fig. 12. SGDBR laser LIV curve (with CW current source) measured by using the SOA 1 as a photodiode.

different components by wet etching to provide some electrical isolation. To reduce parasitic pad capacitance for the high-speed SOA and modulators, photosensitive Benzocyclobutene (BCB) was used in such regions. Ti/Pt/Au was deposited for p contacts. Next, the fabricated samples were thinned to less than 180-μm thickness and backside Ti/Pt/Au n-metal was deposited on the thinned wafers. The cleaved PICs were then solder mounted to ceramic carriers and wire-bonded for characterization.

IV. OFFSET QUAMTUM WELL-BASED TRANSMITTER

The fabricated OQW-based PIC transmitter is shown in Fig. 9. It consists of a widely tunable SGDBR laser, a high-speed SOA (SOA 1), a MZM and a high-power two-section output booster SOA (SOA 2). The waveguide at the output is angled with respect to the chip facet to reduce the reflectivity of this interface. The transmitter has a footprint of 5.5 mm × 0.36 mm. The microscope images at various stages of the fabrication process are demonstrated in Fig. 10.

The five-section widely tunable SGDBR laser consists of an active gain section, a front SGDBR mirror, a back SGDBR mirror, a phase section, and a rear absorber (see Fig. 11). The SGDBR laser has a five-period front sampled grating mirror with 4-μm wide bursts and 68.5-μm period, a 12-period back sampled graing mirror with 6-μm wide bursts and 61.5-μm period [42].

To measure the light-current-voltage (LIV) characteristics, the reversed-biased high-speed integrated SOA (SOA 1) was used as an on-chip photodetector (estimated responsivity 0.9 A/W). The LIV curve of the SGDBR laser is shown in Fig. 12, demonstrating a threshold current of 45 mA and an output optical power of 15 mW at a gain section current of 100 mA. Laser spectrum near 1550 nm is shown in Fig. 13, the side mode suppression ratio (SMSR) is 55 dB. The tuning characteristics of the SGDBR laser are illustrated in Fig. 14 and Fig. 15, which present the emission wavelength and SMSR at various tuning conditions. Fig. 15 shows the 'supermode' boundaries and suggests that the width of the SMSR degradation between switching modes is very small. By adjusting the injected current in the front and back mirrors, the emission wavelength was tuned from 1521 nm to 1565 nm, covering more than the entire C-band. Across the entire tuning range, > 45 dB SMSR was maintained.

There are two SOAs in this transmitter: a high-speed SOA (SOA 1) for amplification/modulation and a two-section booster SOA (SOA 2) with curved/angled and flared ridge waveguides. SOA 1 is 3 μm wide and 400 μm long. It is placed after the laser and before the 1-mm long MZM, and could also be used for modulation. Fig. 16 shows the gain characteristics of the
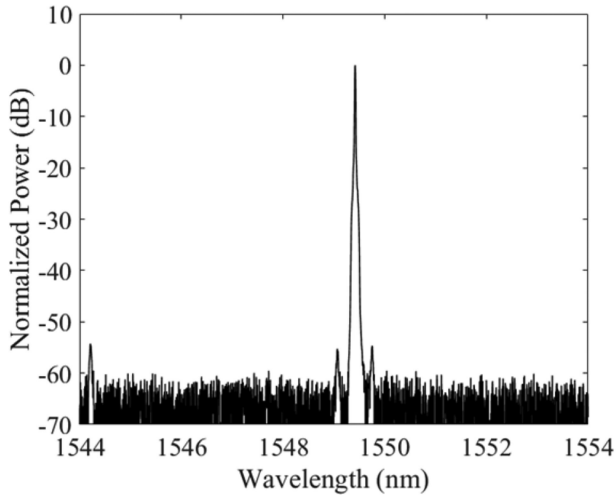
Fig. 13.   Lasing spectrum near 1550 nm with a 55-dB SMSR measured by an optical spectrum analyzer with a resolution bandwidth of 0.02 nm.
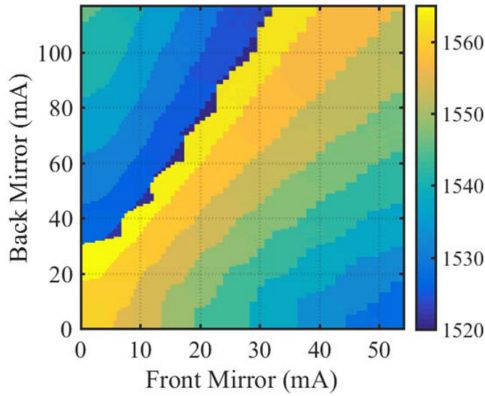

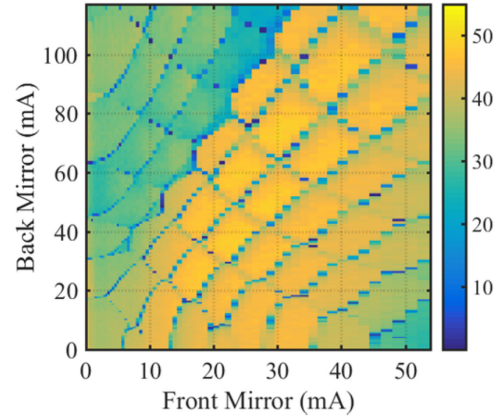Fig. 14.   Emission wavelength (nm) at various tuning conditions.

Fig. 15.   Side mode suppression ratio (dB) at various tuning conditions.
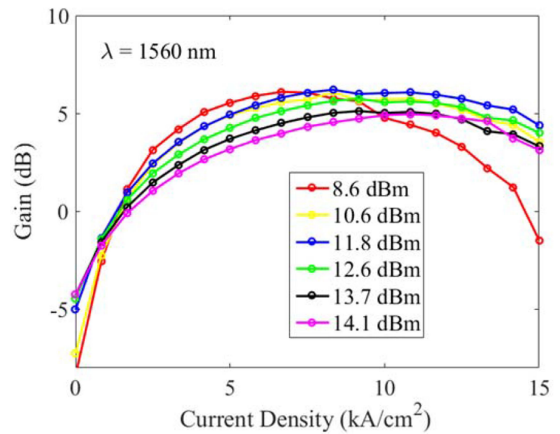

Fig. 16.   Gain as a function of current density for the high-speed SOA (3 μm × 400 μm) with different input power levels at a wavelength of 1560 nm.

high-speed SOA at different input power levels. A gain of 6 dB is achieved at a current density of 10 kA/cm^2, which is sufficient to compensate for the modulator insertion loss. The output booster SOA (SOA 2) is constructed with two separate sections that can be pumped with different injection current levels. The lengths of the two sections are 350 and 500 μm, respectively. The first section is 3-μm wide and the second section linearly flares from 3-μm to 5-μm wide.

The optical output was coupled to an integrating sphere to measure the off-chip power. Fig. 17 shows the off-chip power versus the current density in the flared-waveguide section of SOA 2. The current of the laser gain section, the SOA 1, and the first section of the SOA 2 are 150 mA, 110 mA and 90 mA, respectively. The maximum output power with the above DC biasing is 14.5 dBm (28 mW).

To measure the high-speed performance of the OQW-based transmitter, one arm of the MZM was wire bonded to a 50-Ω RF feeding transmission line and on the other side to a 50-Ω load mounted to the ceramic carrier. Fig. 18 shows the eye diagrams from 2 Gps to 7 Gbps non-return-to-zero (NRZ) on-off keying

(OOK) modulation at a reverse bias of −2.2 V and 3 V signal amplitude (V$_{pp}$).

V. QUANTUM WELL INTERMIXING-BASED TRANSMITTER

Fig. 19 demonstrates the schematic of a high-power transmitter integrated with ultralow-confinement SOA design. The full transmitter contains two stages: stage 1 consists of a laser, an EAM and two SOAs (SOA 1 and SOA 2) with relatively high confinement (Γ = 3% ∼ 4%); Stage 2 features with a transition gain section (SOA 3), and an ultralow-confinement SOA (SOA 4). In stage 1, different elements are integrated by QWI. Transition gain section in stage 2 is a simple linear width taper. The integration of SOA 3 and SOA 4 will just add one additional etch process.

Since the epitaxial structure S2 was optimized for high-power SOA, the performance of laser and EAM may be degraded with the same material. Therefore, our first step is to test the performance of Stage 1, which is similar to the OQW-based transmitter in Sec. IV. Fig. 20 shows the microscope image of the fabricated PIC transmitter, which has a footprint of 3.5 mm × 0.36 mm. It consists of a DBR laser, a high-speed SOA (SOA 1), an EAM,
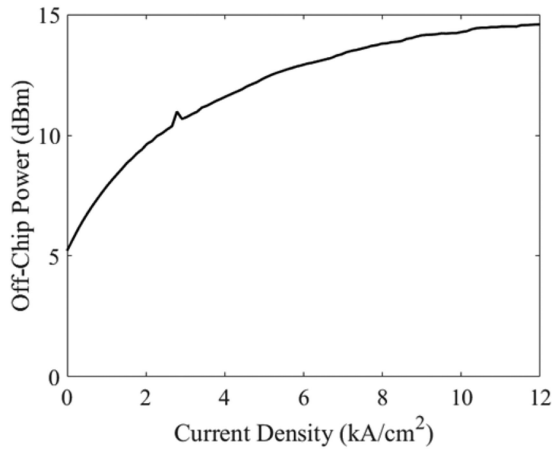
Fig. 17. Off-chip optical power of the PIC transmitter versus the current density in the second section of the booster SOA.
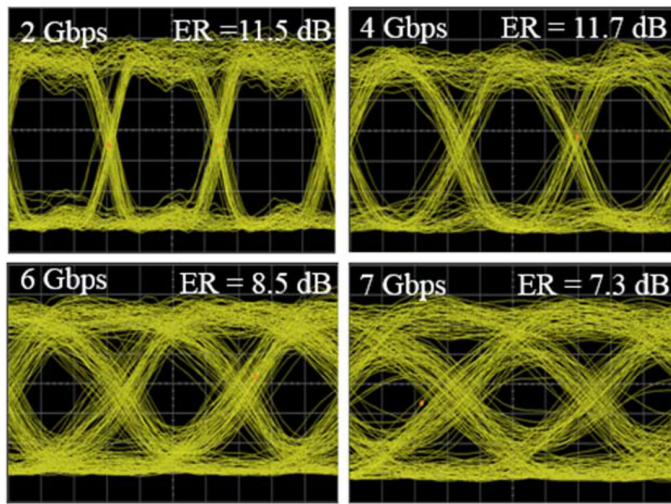

Fig. 21. SEM images at various stages of the fabrication process: (a) The dry-etched ridge waveguide; (b) Passivation etch for modulators; (c) N metal deposition; (d) Isolation between the back mirror and the phase section.

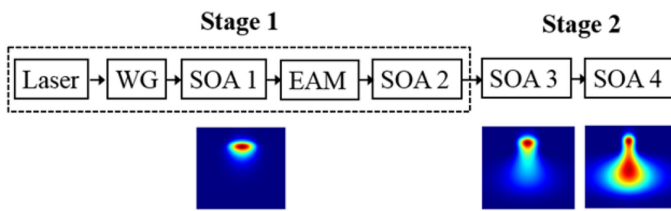Fig. 18. Eye diagrams of OQW-based transmitter with NRZ OOK modulation at a data rate up to 7 Gbps.

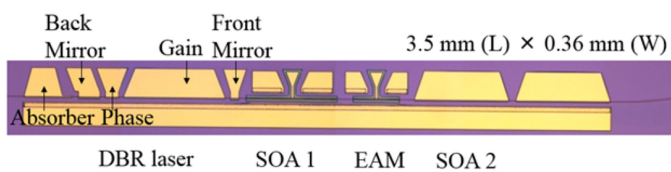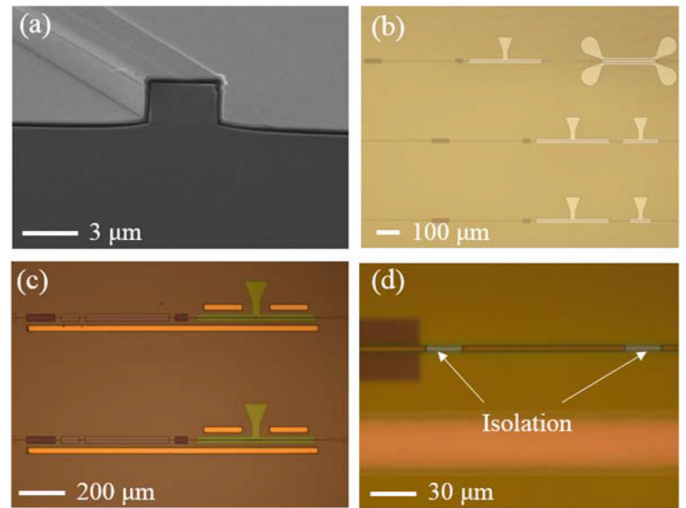Fig. 19. Schematic of a high-power PIC transmitter with integrated ultralow-confinement SOA design.
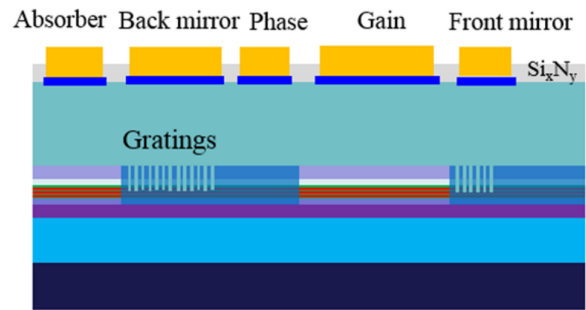
Fig. 22. Schematic of the five-section DBR laser.

Fig. 20. Microscope image of fabricated QWI-based PIC transmitter comprising of a five-section DBR laser, a 250-μm long EAM, and two high-power two-section output booster SOA (SOA 2).

and a high-power two-section output booster SOA (SOA 2). The images at various stages of the fabrication process are shown in Fig. 21.

The DBR laser consists of a rear absorber, a back DBR mirror, a phase section, an active gain section, and a front DBR mirror. The lengths of the front and back mirrors are 50 μm and 120 μm, respectively. The lengths are longer than DBR designs with a conventional high confinement epitaxial structure. In conventional structure, the grating etch will not significantly alter the optical modes, so a deep etch can be performed to achieve high coupling efficiency (κ). The reflectivity of the grating can be written as:

$$r_g = \tanh(\kappa L_g) \tag{3}$$

where L_g is the length of the grating mirror. With high κ, higher reflectivity can be achieved, thus reducing the loss in the mirror. However, in the QWI-based transmitter if the quantum well layers were all etched off, the optical mode would "leak" into the thick waveguide layer (WG2) and result in extra loss (see Fig. 5). Therefore, the etch depth into the quantum wells should be well controlled. In this case, the QWs were only partially etched (as shown in Fig. 22).

Fig. 23.　DBR laser LIV curve (with CW current source) measured by using the SOA 1 as a photodiode.

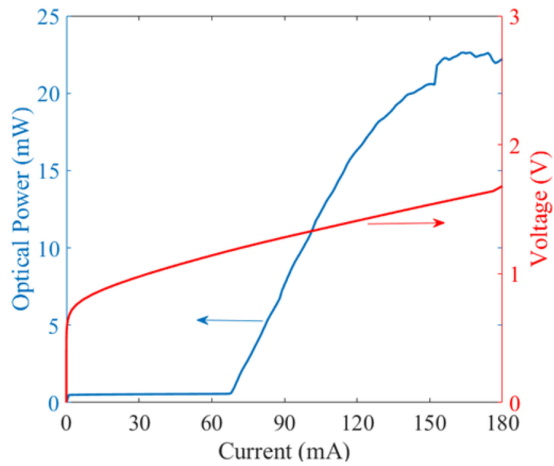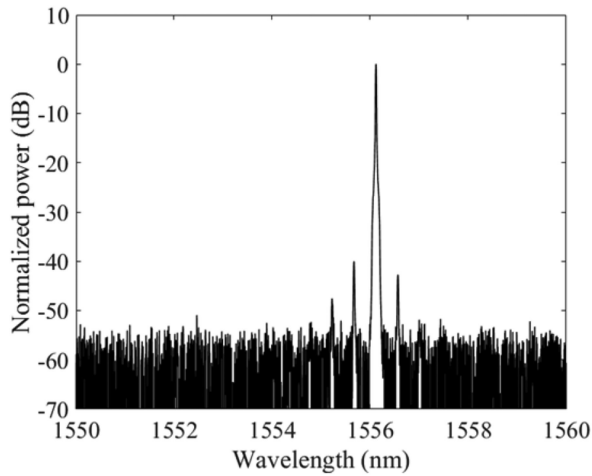Fig. 25.　Gain of SOA 2 as a function of current density in the second section as the current in the first section is increased from 20 to 180 mA.

Fig. 24.　Lasing spectrum near 1556 nm with a 40-dB SMSR measured by an optical spectrum analyzer with a resolution bandwidth of 0.02 nm.

Fig. 26.　Off-chip optical power of the PIC transmitter versus the current density in the second section of the booster SOA.

The LIV characteristic of the DBR laser is plotted in Fig. 23, measured by exploiting the reverse bias SOA 1 as photodetector, which shows a threshold of 65 mA. At a current of 150 mA, the optical power is 20 mW. The SMSR near 1556 nm is 40 dB (see Fig. 24).

SOA1 and each section of SOA 2 are 3-μm wide and 500-μm long. To test the gain characteristic, the laser gain section is biased at 150 mA and SOA 1 at 90 mA. Gain of SOA 2 as a function of the current density in the second section of SOA 2 is plotted in Fig. 25. Here the jumps in the measured SOA gain are ascribed to thermal crosstalk induced mode hopping of the laser.

Fig. 26 shows the off-chip power versus the current density in the second section of the booster SOA (SOA 2). The current of the laser gain section, the SOA 1, and the first section of the SOA 2 are 150 mA, 90 mA and 140 mA, respectively. The maximum output power with the above DC biasing is 19.4 dBm (87 mW). Fig. 27 shows the eye diagram for NRZ OOK modulation up to 20 Gbps.
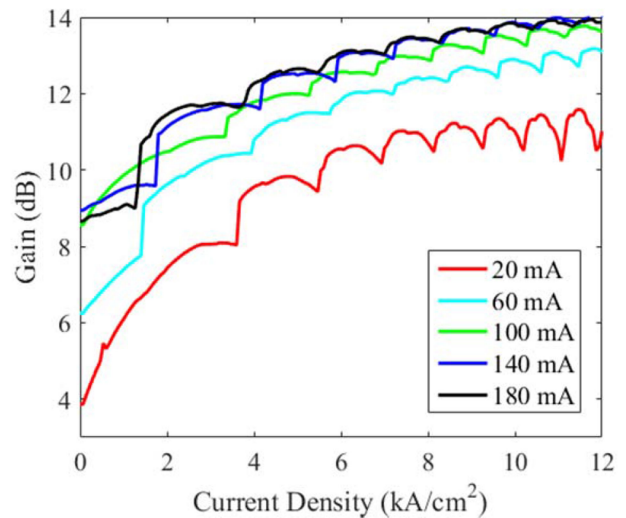

Fig. 27.　Eye diagrams of QWI-based transmitter with NRZ OOK modulation at a data rate up to 20 Gbps.
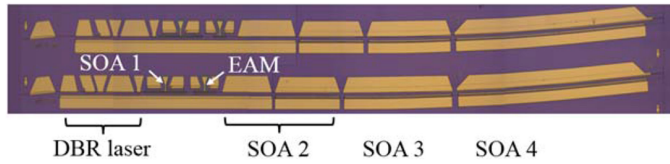
Fig. 28. Microscope image of high-power PIC transmitters with integrated ultralow-confinement SOAs.

Compared with the OQW-based transmitter, the QWI-based one demonstrated both higher optical power and higher data rate, the first enabled by an optimized epi structure, while the second achieved through a compact and efficient EAM. In future work, the fabricated high-power PIC transmitter with integrated ultralow confinement SOA will be characterized. As shown in Fig. 28, the footprint of each transmitter is 8 mm × 0.36 μm. With the ultralow-confinement SOA at the output, >25 dBm off-chip optical power is expected.

VI. CONCLUSION

In this work, InP-based PIC transmitters were fabricated and characterized for high optical output power. The OQW-based transmitter is tunable from 1521 nm to 1565 nm while maintaining >45 dB SMSR across this range. Measured off-chip power of 14.5 dBm and 7-Gbps data rate were demonstrated. A QWI-based transmitter with new epitaxial structure was employed for higher optical output power, which shows 19.5 dBm output power and up to 20 Gbps operation. The new epitaxial material enables ultralow confinement SOA designs and monolithic integration of the SOA with DBR laser, EAM, and passive waveguide.

REFERENCES

[1] L. A. Coldren *et al.*, "High performance InP-based photonic ICs—A tutorial," *J. Lightw. Technol.*, vol. 29, no. 4, pp. 554–570, Feb. 2011.

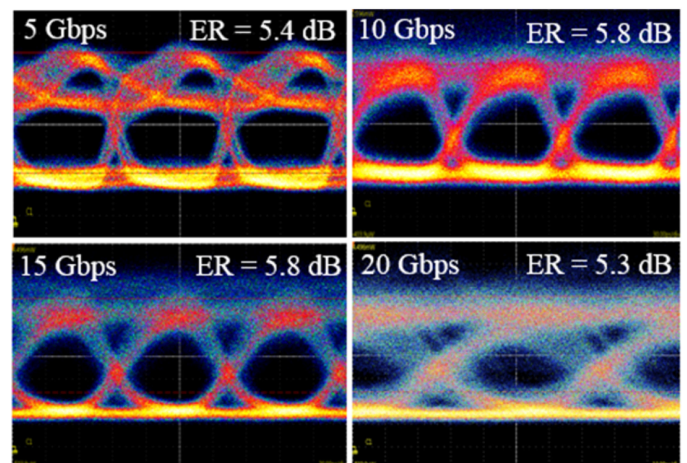[2] D. F. Welch *et al.*, "Large-scale InP photonic integrated circuits: Enabling efficient scaling of optical transport networks," *IEEE J. Sel. Top. Quantum Electron.*, vol. 13, no. 1, pp. 22–31, Jan./Feb. 2007.

[3] J. Klamkin *et al.*, "Indium phosphide photonic integrated circuits: Technology and applications," in *Proc. IEEE BiCMOS Compound Semicond. Integr. Circuits Technol. Symp.*, 2018, pp. 8–13.

[4] T. Koch and U. Koren, "Semiconductor lasers for coherent optical fiber communications," *J. Lightw. Technol.*, vol. 8, no. 3, pp. 274–293, Mar. 1990.

[5] M. M. Dummer, J. Klamkin, A. Tauke-Pedretti, and L. A. Coldren, "40 Gb/s field-modulated wavelength converters for all-optical packet switching," *IEEE J. Sel. Topics Quantum Electron.*, vol. 15, no. 3, pp. 494–503, May/Jun. 2009.

[6] S. C. Nicholes *et al.*, "The world's first InP 8 × 8 monolithic tunable optical router (MOTOR) operating at 40 Gbps line rate per port," in *Proc. Conf. Opt. Fiber Commun.*, 2009, Paper PDPB1.

[7] J. Summers *et al.*, "40 Channels × 57 Gb/s monolithically integrated InP-based coherent photonic transmitter," in *Proc. Eur. Conf. Opt. Commun.*, 2014, Paper P.2.5.

[8] Y. Kawamura, K. Wakita, Y. Yoshikuni, Y. Itaya, and H. Asahi, "Monolithic integration of a DFB laser and an MQW optical modulator in the 1.5 μm wavelength range," *IEEE J. Quantum Electron.*, vol. QE-23, no. 6, pp. 915–918, Jun. 1987.

[9] M. Suzuki *et al.*, "Monolithic integration of InGaAsP/InP distributed feedback laser and electroabsorption modulator by vapor phase epitaxy," *J. Lightw. Technol.*, vol. LT-5, no. 9, pp. 1277–1285, Sep. 1987.

[10] E. J. Skogen *et al.*, "Widely tunable negative-chirp SG-DBR laser/EA-modulated transmitter," *J. Lightw. Technol.*, vol. 23, no. 1, pp. 80–86, Jan. 2005.

[11] L. A. Coldren, "Monolithic tunable diode lasers," *IEEE J. Sel. Topics Quantum Electron.*, vol. 6, no. 6, pp. 988–999, Nov./Dec. 2000.

[12] V. Jayaraman, Z. M. Chuang, and L. A. Coldren, "Theory, design, and performance of extended tuning range semiconductor lasers with sampled gratings," *IEEE J. Quantum Electron.*, vol. 29, no. 6, pp. 1824–1834, Jun. 1993.

[13] R. Nagarajan *et al.*, "Large-scale photonic integrated circuits," *IEEE J. Sel. Top. Quant. Electron.*, vol. 11, no. 1, pp. 50–65, Jan./Feb. 2005.

[14] V. Lal *et al.*, "Extended C-band tunable multi-channel InP-based coherent transmitter PICs," *J. Lightw. Technol.*, vol. 35, no. 7, pp. 1320–1327, Apr. 2017.

[15] H. Zhao *et al.*, "Indium phosphide photonic integrated circuits for free space optical links," *IEEE J. Sel. Top. Quant. Electron.*, vol. 24, no. 6, Nov./Dec. 2018, Art. no. 6101806.

[16] H. Zhao *et al.*, "Integrated indium phosphide transmitter for free space optical link," in *Proc. Adv. Photon.*, 2018, Paper ITu4B.6.

[17] S. Iezekiel, M. Burla, J. Klamkin, D. Marpaung, and J. Capmany, "RF engineering meets optoelectronics: Progress in integrated microwave photonics," *IEEE Microw. Mag.*, vol. 16, no. 8, pp. 28–45, Sep. 2015.

[18] J. A. Nanzer, A. Wichman, J. Klamkin, T. P. McKenna, and T. R. Clark, "Millimeter-wave photonics for communications and phased arrays," *Fiber Integr. Opt.*, vol. 34, no. 4, pp. 159–174, Jul. 2015.

[19] A. Ramaswamy *et al.*, "Integrated coherent receivers for high-linearity microwave photonic links," *J. Lightw. Technol.*, vol. 26, no. 1, pp. 209–216, Jan. 2008.

[20] S. Arafin *et al.*, "Towards chip-scale optical frequency synthesis based on optical heterodyne phase-locked loop," *Opt. Express*, vol. 25, no. 2, pp. 681–695, 2017.

[21] B. Isaac *et al.*, "Indium phosphide photonic integrated circuit transmitter with integrated linewidth narrowing for laser communications and sensing," presented at the IEEE Int. Semicond. Laser Conf., Santa Fe, NM, USA, 2018, Paper MC.5.

[22] M. A. Krainak and A. W. Yu, "1047-nm master oscillator power amplifier free-space optical communications laser transmitter," *IEEE J. Quantum Electron.*, vol. 32, no. 1, pp. 112–117, Jan. 1996.

[23] D. O. Caplan, "Laser communication transmitter and receiver design," *J. Opt. Fiber Commun.* vol. 4, pp. 225–362, 2007.

[24] H. Hemmati, A. Biswas, and I. B. Djordjevic, "Deep-space optical communications: Future perspectives and applications," *Proc. IEEE*, vol. 99, no. 11, pp. 2020–2039, Aug. 2011.

[25] H. Zhao *et al.*, "Widely tunable integrated laser transmitter for free space optical communications," presented at the IEEE Int. Semicond. Laser Conf., Santa Fe, NM, USA, 2018, Paper MC.5.

[26] D. M. Boroson, J. J. Scozzafava, D. V. Murphy, B. S. Robinson, and M. I. T. Lincoln, "The lunar laser communications demonstration (LLCD)," in *Proc. 3rd IEEE Int. Conf. Space Mission Challenges Inf. Technol.*, 2009, pp. 23–28.

[27] D. J. Israel, B. L. Edwards, and J. W. Staren, "Laser communications relay demonstration (LCRD) update and the path towards optical relay operations," in *Proc. IEEE Aerosp. Conf.*, 2017, pp. 1–6.

[28] D. Caplan, "High-performance free-space laser communications and future trends," presented at the Opt. Amplifiers Their Appl., 2005, Paper TuB1.

[29] H. Zhao *et al.*, "High-power integrated indium phosphide transmitter for free space optical communications," presented at the IEEE Conf. Lasers Electro-Optics (CLEO), 2018, Paper JW2A.52.

[30] P. W. Juodawlkis *et al.*, "High-power, low-noise 1.5-μm slab-coupled optical waveguide (SCOW) emitters: Physics, devices, and applications," *IEEE J. Sel. Top. Quant. Electron.*, vol. 17, no. 6, pp. 1698–1714, Nov./Dec. 2011.

[31] J. Klamkin *et al.*, "High-output saturation power variable confinement slab-coupled optical waveguide amplifier," presented at the Opt. Fiber Commun. Conf. /Nat. Fiber Optic Eng. Conf., Los Angeles, CA, USA, 2011, Paper JThA025.

[32] M. Faugeron *et al.*, "High power three-section integrated master oscillator power amplifier at 1.5 μm," *IEEE Photon. Technol. Lett.*, vol. 27, no. 13, pp. 1449–1452, Jul. 2015.

[33] J. P. Donnelly *et al.*, "High-power 1.3-μm InGaAsP-InP amplifiers with tapered gain regions," *IEEE Photon. Technol. Lett.*, vol. 8, no. 11, pp. 1450–1452, Nov. 1996.

[34] G. Bendeli, K. Komori, S. Arai, and Y. Suematsu, "A new structure for high power TW-SLA (Travelling wave semiconductor laser amplifier)," *IEEE Photon. Technol. Lett.*, vol. 3, no. 1, pp. 42–44, Jan. 1991.

[35] F. Koyama, K.-Y. Liou, A. G. Dentai, T. Tanbun-ek, and C. A. Burrus, "Multiple-quantum-well GaInAs/GaInAsP tapered broad-area amplifiers with monolithically integrated waveguide lens for high-power applications," *IEEE Photon. Technol. Lett.*, vol. 5, no. 8, pp. 916–919, Aug. 1993.

[36] J. J. Plant *et al.*, "1.5-μm InGaAsP-InP slab-coupled optical waveguide lasers," *IEEE Photon. Technol. Lett.*, vol. 17, no. 4, pp. 735–737, Apr. 2005.

[37] J. Klamkin *et al.*, "Direct modulation and wavelength stabilization of high power slab-coupled optical waveguide lasers," in *Proc. Conf. Lasers Electro-Opt.*, 2010, Paper CWE4.

[38] M. Aoki *et al.*, "Novel structure MQW electroabsorption modulator/DFB-laser integrated device fabricated by selective area mocvd growth," *Electron. Lett.*, vol. 27, no. 23, pp. 2138–2140, 1991.

[39] T. Tanbun-Ek *et al.*, "DFB lasers integrated with Mach-Zehnder opticalmodulator fabricated by selective area growth MOVPE technique," *IEEE Photon. Technol. Lett.*, vol. 7, no. 9, pp. 1019–1021, Sep. 1995.

[40] B. Mason *et al.*, "40-Gb/s tandem electroabsorption modulator," *IEEE Photon. Technol. Lett.*, vol. 14, no. 1, pp. 27–29, Jan. 2002.

[41] J. J. M. Binsma *et al.*, "MOVPE waveguide regrowth in InGaAsP/InP with extremely low butt-joint loss," in *Proc. Annu. Symp. IEEE/LEOS*, 2001, pp. 245–248.

[42] M. Smit *et al.*, "An introduction to InP-based generic integration technology," *Semicond. Sci. Technol.*, vol. 29, no. 8, Jun. 2014, Art. no. 083001.

[43] L. M. Augustin *et al.*, "InP-based generic foundry platform for photonic integrated circuits," *IEEE J. Sel. Topics Quantum Electron.*, vol. 24, no. 1, Jan./Feb. 2018, Art. no. 6100210.

[44] J. S. Barton, "The integration of Mach-Zehnder modulators with sampled grating DBR lasers," Ph.D. dissertation, Elect. Comput. Eng., University of California Santa Barbara, Santa Barbara, CA, USA, 2004.

[45] A. M. Tauke-Pedretti, "Monolithic separate absorption and modulation Mach-Zehnder wavelength converters," Ph.D. dissertation, Elect. Comput. Eng., University of California Santa Barbara, Santa Barbara, CA, USA, 2007.

[46] E. J. Skogen, J. S. Barton, S. P. DenBaars, and L. A. Coldren, "A quantum-well-intermixing process for wavelength-agile photonic integrated circuits," *IEEE J. Sel. Top. Quant. Electron.*, vol. 8, no. 4, pp. 863–869, Jul./Aug. 2002.

[47] J. J. Plant *et al.*, "Compact external-cavity semiconductor mode-locked laser with quantum-well-intermixed modulator and saturable absorber," in *Proc. IEEE Photon. Soc. 24th Annu. Meeting*, Arlington, VA, USA, 2011, Paper ThK3.

Hongwei Zhao received the B.S. degree from the Huazhong University of Science and Technology, Wuhan, China, in 2008, and the M.S. degree from the Institute of Semiconductors, Chinese Academy of Sciences, Beijing, China, in 2011. She is currently working toward the Ph.D. degree in the Integrated Photonics Lab, Electrical and Computer Engineering Department, University of California Santa Barbara, Santa Barbara, CA, USA. Her research interests include silicon photonics with emerging materials (such as graphene, indium tin oxide, and indium silicon oxide), compound semiconductor photonic integrated circuits, InP-based photonic integrated circuits for free space communications, and monolithic integration of III-V lasers on Si substrate.

Sergio Pinna received the B.Sc. and M.Sc. degrees in telecommunications engineering from University of Pisa, Pisa, Italy, and the Ph.D. degree in innovative technologies from Scuola Superiore Sant'Anna, Pisa, Italy, in 2008, 2010, and 2014, respectively. From November 2010 to December 2015, he was a Fellow with CNIT, National Photonic Networks Laboratory, Pisa, Italy. In 2014, he was a Visiting Researcher with the Integrated Photonics Laboratory, Boston University, Boston, MA, USA. Since January 2016, he has been a Research Fellow with TeCIP Institute, Scuola Superiore Sant'Anna, Pisa, Italy, within the Digital and Microwave Photonics Group. In 2017, he joined the Integrated Photonics Laboratory, University of California Santa Barbara, as a Postdoctoral Research Associate. His research interests include integrated photonics for microwave and LiDAR applications.

Fengqiao Sang received the B.S. degree in electrical engineering from Drexel University, Philadelphia, PA, USA. He is currently working toward the Ph.D. degree in the Electrical and Computer Engineering Department, University of California Santa Barbara, Santa Barbara, CA, USA. His research interests include photonic integrated circuits and semiconductor lasers.

Bowen Song is from Shanxi, China. He received the Bachelor of Engineering degree from the School of Electronic Engineering and Optoelectronic Technology, Nanjing University of Science and Technology, Nanjing, China, in 2012, and the Master of Science degree in developing nano-patterned sapphire substrate for AlGaN-based deep UV LEDs from Wide Bandgap Semiconductor Laboratory, Boston University, Boston, MA, USA, in 2014. He is currently working toward the Ph.D. degree in the Electrical and Computer Engineering Department, University of California Santa Barbara, Santa Barbara, CA, USA. His research interests include electronic-photonic integration, integrated photonics, and integrated LiDAR.

Simone Tommaso Šuran Brunelli received the bachelor's degree in industrial engineering and the master's degree in materials engineering from the Università degli Studi di Trieste, Trieste, Italy. After a fellowship at Elettra Sincrotrone, working on carbon nanotube synthesis and photoelectron spectroscopy, he joined the Integrated Photonics Laboratory, University of California Santa Barbara, Santa Barbara, CA, USA, as a Ph.D. student. His current research focuses on metal organic chemical vapor deposition of III-V semiconductors for nanoelectronic and photonic applications including low-power tunneling transistors.

Larry A. Coldren (S'67–M'72–SM'77–F'82–LF'12) received the Ph.D. degree in electrical engineering from Stanford University, Stanford, CA, USA, in 1972. After 13 years in the research area with Bell Laboratories, he joined the University of California at Santa Barbara (UCSB), CA, USA, in 1984. He is currently the Fred Kavli Professor of optoelectronics and sensors and holds appointments with the Department of Materials and the Department of Electrical and Computer Engineering, University of California Santa Barbara. From 2009 to 2011, he was the acting as Dean of the College of Engineering, University of California Santa Barbara. In 1990, he cofounded Optical Concepts, later acquired as Gore Photonics, to develop novel VCSEL technology, and, in 1998, he cofounded Agility Communications, later acquired by JDSU (now Lumentum), to develop widely tunable integrated transmitters. At UCSB, he worked on multiple-section widely tunable lasers and efficient vertical-cavity surface-emitting lasers (VC-SELs). More recently, his group has developed high-performance InP-based photonic integrated circuits and high-speed, high-efficiency VCSELs. He has authored or coauthored more than a thousand journal and conference papers, eight book chapters, a widely used textbook, and 63 issued patents. He is a Fellow of OSA, and the National Academy of Inventors, as well as a member of the National Academy of Engineering. He was the recipient of the 2004 John Tyndall Award, the 2009 Aron Kressel Award, the 2014 David Sarnoff Award, the 2015 IPRM Award, and the 2017 Nick Holonyak, Jr. Award.

Jonathan Klamkin (SM'15) received the B.S. degree from Cornell University, Ithaca, NY, USA, and the M.S. and Ph.D. degrees from the University of California Santa Barbara (UCSB), Santa Barbara, CA, USA. From 2008 to 2011, he was a member of the Technical Staff in the Electro-Optical Materials and Devices Group, MIT Lincoln Laboratory, Lexington, MA, USA. From 2011 to 2013, he was an Assistant Professor with the Institute of Communication, Information and Perception Technologies, Scuola Superiore Sant'Anna, Pisa, Italy. From 2013 to 2015, he was an Assistant Professor of Electrical and Computer Engineering (ECE) and Materials with Boston University, Boston, MA, USA. In 2015, he joined the ECE Department, University of California Santa Barbara, where he is currently an Associate Professor and Director of the UCSB Nanotech. He has authored or coauthored more than 180 journal and conference papers, and holds three patents. He is an Associate Editor of *Photonics Technology Letters*, Vice Chair of the Microwave Theory and Techniques Society Subcommittee on Microwave Photonics, and Steering Committee Member of the *Journal of Lightwave Technology*. He was the Program Chair of the Integrated Photonics Research, Silicon and Nanophotonics Conference, in 2017, and the General Chair of the same conference, in 2018. He or his group members were the recipient of best paper awards at the 2006 Conference on Optoelectronic and Microelectronic Materials and Devices, 2007 Microwave Photonics Conference, and 2017 Asia Communications and Photonics Conference. He was the recipient of the NASA Early Career Faculty Award and the DARPA Young Faculty Award. He is a Senior Member of OSA.